Total transmission and total reflection by zero index metamaterials with defects

Viet Cuong Nguyen,[1] Lang Chen,[1,*] and Klaus Halterman[2]

[1] *50 Nanyang Avenue, School of Materials Science and Engineering Nanyang Technological University, Singapore 639798, Singapore.*

[2] *Research and Intelligence Department, Physics Division, Naval Air Warfare Center, China Lake, California 93555*

In this Letter, we theoretically investigate microwave transmission through a zero-index metamaterial loaded with dielectric defects. The metamaterial is impedance matched to free space, with the permittivity and permeability tending towards zero over a given frequency range. By simply varying the radii and permittivities of the defects, *total* transmission or reflection of the impinging electromagnetic wave can be achieved. The proposed defect-structure can offer advances in shielding or cloaking technologies without restricting the object's viewpoint. Active control of the observed exotic transmission and reflection signatures can occur by incorporating tunable refractive index materials such as liquid crystals and BaSr TiO_3.

The field of metamaterials continues to flourish and evolve, in part due to the recent interest and excitement arising from potential applications involving invisibility cloaking [1, 2], perfect lenses [3], and slow light devices [4]. One of the primary thrusts of metamaterials is the design of electromagnetic (EM) structures that have a prescribed response to the incident electric (**E**) and magnetic (**H**) fields, characterized by the permittivity, ϵ, and permeability, μ. The vast number of metamaterials are structures consisting of double negative index media (real parts of ϵ and μ are negative) [5], single negative index media (real part of ϵ or μ is negative) [6], epsilon zero media (EZM) (real part of ϵ is zero), and matched impedance zero index material (MIZIM), where ϵ and μ both vanish over a narrow frequency window [7, 8]. Compared with the widely popular double negative index and single negative index materials, zero index metamaterials (ZIMs), whose permittivity and permeability are simultaneously or individually equal to zero, has received much less attention. As the experimental landscape is continually refined, many of these theoretical concepts once viewed as high-risk appear within grasp.

Structures involving ZIMs have been investigated experimentally and theoretically by several scientists [8–16]. The tunneling of EM waves through ultranarrow ZIM channels has been demonstrated experimentally in the RF regime [11, 12]. Moreover, a subwavelength ZIM slit can result in strong transmission of EM waves differing from conventional Fabry-Perot resonances [14]. The infrared transmission and reflectivity measurements taken long ago [15] of silicon carbide (SiC), indicated a near zero index of refraction. The fabrication of metallo-dielectric ZIMs in the microwave regime was reported [17], and a stacked Drude checkerboard structure was created for IR wavelengths [18]. If the ZIM is impedance matched to free space, where μ also vanishes, the corresponding matched impedance zero index material (MIZIM) can exhibit more dramatic properties. The idea of MIZIM slabs as perfect lenses was discussed [19], and "nihility" was extended later to scattering by MIZIM cylinders and spheres [20]. It was also shown theoretically that a MIZIM can facilitate total transmission without changing the phase, and act as a transformer that converts small-curvature wave fronts into output beams with planar-like wave fronts [16]. As investigations into the full phenomena that can arise in MIZIMs is still incomplete, there are some limited experimental results, including successful fabrication of a mid-IR MIZIM [21].

Our aim is to reveal how total reflection *and* total transmission of an EM wave can occur by simply controlling the geometrical and material properties of certain "defects", consisting of either conventional dielectric rods (such as FR4) or low loss high-dielectric materials (like $MgCaTiO_3$ or $BaTiO_3$) arbitrarily embedded in a MIZIM. The irrotational electric and magnetic fields in the MIZIM permits complimentary analytical and numerical solutions to Maxwell's equations. Perfect transmission or reflection can be exploited through variations in either the radius R of the defect, the frequency of the wave, or the constitutive material values of the defects. It is also shown that considerable field enhancement can arise in extreme-dielectric defects. Finally, we discuss a few of the possible applications for our proposed system, including invisibility and perfect shielding.

We consider an EM wave incident from the left into the structure illustrated in Fig. 1. The **H** field is polarized in the z direction, and the **E** field is y-directed. For simplicity, we consider the fundamental TEM mode [7]. The central MIZIM layer is a Drude-like material with permittivity, $\epsilon_1 = 1 - \omega_p^2/[\omega(\omega + i\Gamma)]$, and permeability, $\mu_1 = 1 - \omega_p^2/[\omega(\omega + i\Gamma)]$. The plasma frequency is ω_p, and Γ is related to the mean free path. In the microwave regime, we have $f_p \equiv \omega_p/(2\pi) = 15$ GHz. The surrounding free space layers correspond to regions 0 and 3. The defects in region 2 that are embedded in MIZIM consist of N cylinders with the permittivity and permeability of the ith cylinder ($i = 1, 2, 3, \ldots, N$) equal to $\epsilon_{2,i}$ and $\mu_{2,i}$ respectively. We assume an $\exp(-i\omega t)$ time dependence throughout, where ω is the usual angular frequency. The EM wave in each region must satisfy

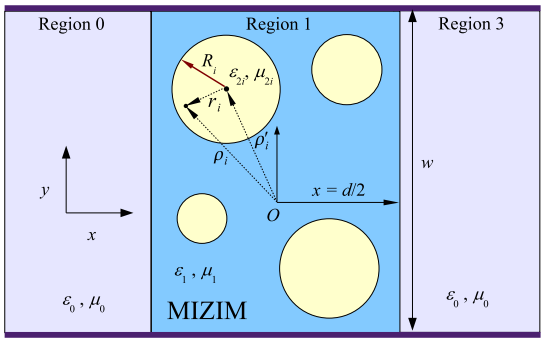

FIG. 1. (Color online) Schematic of the proposed vacuum-MIZIM-vacuum metamaterial structure containing an arbitrary arrangement of N defects (region 2). The propagation direction of the EM wave is along the x-axis. The central MIZIM layer (with ϵ_1 and μ_1) in region 1 has thickness d in the x direction and width w in the y direction. The ith cylindrical defect has radius R_i, permittivity $\epsilon_{2,i}$, and permeability, $\mu_{2,i}$. The upper and lower boundaries correspond to a perfectly conducting metal or perfect magnetic boundary, depending on the polarization of the incident wave.

the Ampére-Maxwell equation,

$$\mathbf{E}_m = \frac{ic}{\omega\epsilon_m}\nabla\times\mathbf{H}_m, \tag{1}$$

where c is the speed of light in vacuum, and the integer m denotes the region. If we consider the MIZIM region for frequencies near ω_p, so that $\mathrm{Re}[\epsilon_1]$ tends to zero (we take $\Gamma = 0$ for now), $\nabla\times\mathbf{H}_1$ must vanish in order to keep the electric field finite [10], resulting in a quasistatic situation. For our z invariant geometry and incident polarization state, this implies that $\nabla H_1^z = 0$, or H_1^z is a constant, which we denote by H_1. Due to this condition, any EM scattering from region 2 will result in a net global shift in the magnetic field of region 1 rather than any local spatial fluctuations. For our configuration, Maxwell's equations demand that the EM field in each region must also obey the vector Helmholtz equation,

$$\left(\frac{\partial^2}{\partial x^2}+\frac{\partial^2}{\partial y^2}+\frac{\omega^2}{c^2}\epsilon_m\mu_m\right)\mathbf{\Psi}_m = 0, \tag{2}$$

where $\mathbf{\Psi}_m \equiv (\mathbf{E}_m, \mathbf{H}_m)$. In the limit of ϵ_m or μ_m vanishing, the Helmholtz equation reduces to the Laplace equation, where quasistatic methods can be utilized. In general we write, $\mathbf{H}_m = \hat{\mathbf{z}}H_m^z(x,y)$, and the electric field as $\mathbf{E}_m = \hat{\mathbf{x}}E_m^x(x,y) + \hat{\mathbf{y}}E_m^y(x,y)$. For the case of plane wave incidence at oblique angles, the use of a ZIM slab as an angular filter has been discussed [7]. For TEM mode excitation, in region 0 the $\mathbf{H}$ field is the sum of incident and reflected waves that satisfy (2),

$$\mathbf{H}_0 = \hat{\mathbf{z}}H_0[e^{ik_0(x+d/2)} + \mathcal{R}e^{-ik_0(x+d/2)}] \tag{3}$$

and from (1), the corresponding electric field is,

$$\mathbf{E}_0 = \hat{\mathbf{y}}H_0[e^{ik_0(x-d/2)} - \mathcal{R}e^{-ik_0(x-d/2)}], \tag{4}$$

where $\mathcal{R}$ is the reflection coefficient, k_0 is the wave vector of free space ($k_0 = \omega/c$), and H_0 is a constant coefficient representing the incident field amplitude. Similarly, in region 3, the magnetic field is written as $\mathbf{H}_3 = \hat{\mathbf{z}}H_0\mathcal{T}\exp(ik_0[x-d/2])$, with corresponding electric field, $\mathbf{E}_3 = \hat{\mathbf{y}}H_0\mathcal{T}\exp(ik_0[x-d/2])$, and where $\mathcal{T}$ is the transmission coefficient. Equating the tangential components of the EM field at the vacuum-MIZIM interfaces, ($x = -d/2$ and $x = d/2$), reveals a simple relationship between the magnetic field coefficients: $(\mathcal{R}+1)H_0 = H_1$, and $\mathcal{T}H_0 = H_1$. For a given arrangement of (non-overlapping) cylindrical defects in the MIZIM, complicated magnetic coupling is avoided, thus permitting a closed form solution to Eq. (2). After implementing Dirichlet boundary conditions at the surface of each defect, we obtain the magnetic field distribution within all N defects,

$$\mathbf{H}_{2,i} = H_1\sum_{i=1}^{N}\frac{J_0(k_{2,i}r_i)}{J_0(k_{2,i}R_i)}\hat{\mathbf{z}}, \tag{5}$$

where J_n is the Bessel function of the first kind and order n, and the wavevector in the ith cylinder, $k_{2,i}$, satisfies the dispersion relation, $k_{2,i} \equiv k_0\sqrt{\epsilon_{2,i}\mu_{2,i}}$. The relative coordinate, r_i, conveniently describe points within each defect via, $r_i = |\boldsymbol{\rho}_i - \boldsymbol{\rho}_i'| = \sqrt{(x_i-x_i')^2+(y_i-y_i')^2}$, where x_i' and y_i' locate the centers of each cylinder relative to the prescribed origin of coordinates (see Fig. 1). It is straightforward to calculate the electric field inside each defect using Eqs. (5) and (1),

$$\mathbf{E}_{2,i} = iH_1\sum_{i=1}^{N}\sqrt{\frac{\mu_{2,i}}{\epsilon_{2,i}}}\frac{J_1(k_{2,i}r_i)}{J_0(k_{2,i}R_i)}\hat{\boldsymbol{\phi}}_i, \tag{6}$$

where $\hat{\boldsymbol{\phi}}_i$ is the azimuthal unit vector for the ith cylinder.

To conveniently determine the transmission features, in the MIZIM without intricate details of the electric field in that region, we employ the Faraday-Maxwell equation, $\mathbf{H}_m = c/(i\omega\mu_m)\nabla\times\mathbf{E}_m$. It is evident from this expression that the as ϵ_1 and μ_1 tend to zero, $\mathbf{E}_1$ becomes irrotational. Subdividing the multiply-connected MIZIM region via the appropriate cuts, and applying Stokes' theorem (integration along infinitesimally close cuts cancel) gives the conservation requirement, $\oint_{\partial C}\mathbf{E}\cdot d\boldsymbol{\ell} + \sum_{i=1}^{N}\oint_{\partial C_{2,i}}\mathbf{E}_{2,i}\cdot d\boldsymbol{\ell} = 0$, where ∂C is the boundary enclosing the whole MIZIM region. After calculating the first line integral above, we we have for the transmission coefficient,

$$\mathcal{T} = \frac{1}{1-\dfrac{1}{2wH_1}\displaystyle\sum_{i=1}^{N}\oint_{\partial C_{2,i}}\mathbf{E}_{2,i}\cdot d\boldsymbol{\ell}_i}, \tag{7}$$

where $\partial C_{2,i}$ denotes the boundary of each defect. Insert-

ing the **E** field (6) gives,

$$\mathcal{T} = \frac{1}{1 - \dfrac{i\pi}{w}\displaystyle\sum_{i=1}^{N}\sqrt{\frac{\mu_{2,i}}{\epsilon_{2,i}}}\frac{R_i J_1(k_{2,i}R_i)}{J_0(k_{2,i}R_i)}}. \tag{8}$$

According to Eq. (8), strong reflection of the incident wave arises if the sum in the denominator diverges (so that $\mathcal{T} \to 0$). In fact, this can occur if only a *single* defect satisfies $J_0(k_{2,i}R_i) = 0$, irregardless of the number of other defects or their material properties, $\epsilon_{2,i}$ and $\mu_{2,i}$. To highlight this phenomenon further, consider Eq. (5), with $k_{2,i}R_i$ chosen such that denominator of (5) is zero. Then on physical grounds, the magnetic field inside region 1 must then vanish to maintain a finite value for $\mathbf{H}_2$. Because the **H** field in region 1 is zero, the EM wave is totally reflected, or, $\mathcal{R} = -1$ [see expression above Eq. (5)]. Thus, one can optimize the system for the many combinations of frequency, defect size, and $\epsilon_{2,i}$ and $\mu_{2,i}$, that yields zeros to $J_0(k_{2,i}R_i)$. A key aspect is that the **E** and **H** fields in the defects are finite. It may be possible to also obtain perfect reflection by coating a cylinder with perfectly magnetic conducting (PMC) layers [22], but at the cost of eliminating the internal defect field.

The denominator in Eq. (8) also reveals how to achieve perfect transmission of EM energy through the structure. By choosing suitable combinations of $k_{2,i}$ and R_i that yield roots to $J_1(k_{2,i}R_i) = 0$ (for all i), $\mathbf{E}_1$ at the boundary between regions 1 and 2 will also be zero. Each term in the summation in Eq. (8) therefore vanishes and perfect transmission ensues. This criteria also ensures that the perfect transmission phenomenon is insensitive to the width d of the MIZIM (see Eq. (8)). This differs from a single ENZ slab, where the transmission varies inversely with the electrical size of the slab [7]. The methodology explored here is easily modified for other polarization states of the incident source wave.

We now compliment our analytical results with numerical simulations from a commercial finite element software package [25]. In what follows we take the spatial domain to have dimensions, $w = 44$ mm, and $d = 60$ mm (for the cases studied here, the results are relatively insensitive to these values). Unless otherwise stated, the excitation source has a frequency of $f = 15$ GHz, and all defects are nonmagnetic ($\mu_{2,i} = 1$). Our investigation first centers around the MIZIM region containing three arbitrarily arranged dielectric defects, each with the proper radii and material parameters to yield perfect reflection. In Fig. 2(a), the magnetic field distribution is shown for defects with radii $R_1 = 4$ mm, $R_2 = 8$ mm, and $R_3 = 12$ mm. The corresponding permittivities are $\epsilon_{2,1} = 3.66$, $\epsilon_{2,2} = 11.86$, and $\epsilon_{2,3} = 15.67$. The plot clearly demonstrates complete reflection of the incident radiation, despite the impedance matching; an unexpected result that holds for even electrically small subwavelength defects ($R_i/\lambda_0 \ll 1$). This is evident

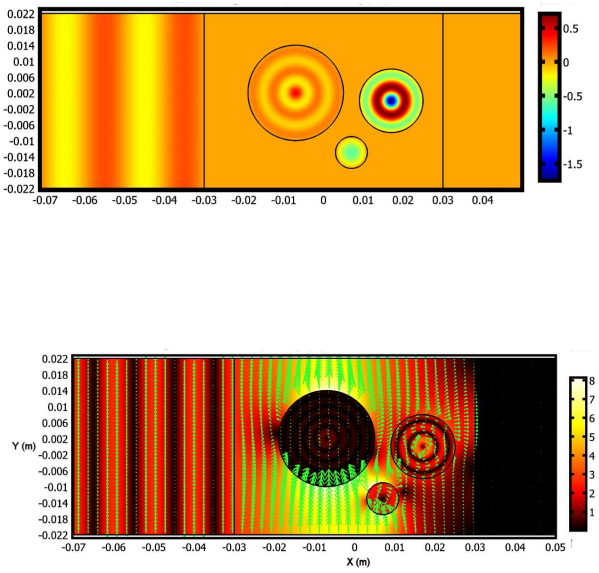

FIG. 2. (Color online) Perfect reflection: (a) the magnetic field distribution for an arrangement of three defects embedded in a MIZIM. The radii are $R_1 = 4$ mm, $R_2 = 8$ mm, and $R_3 = 12$ mm with respective materials, $\epsilon_{2,1} = 3.7$, $\epsilon_{2,2} = 11.9$, and $\epsilon_{2,3} = 15.7$. The **E** field magnitude is shown in (b) with its associated vector field distribution.

by considering the first zero of the Bessel function for a single defect ($i = 1$): $R/\lambda_0 \approx 0.38274/\sqrt{\epsilon_{2,1}\mu_{2,1}}$. In Fig. 2(b), the **E** field is shown for the same parameters in (a). Although both the **E** and **H** field are curl-free in the MIZIM, the electric field exhibits more complicated behavior, since its 2-D polarization state can vary in x and y. As alluded to above, if only one defect is tailored to satisfy $J_0(2\pi\sqrt{\epsilon_{2,i}\mu_{2,i}}R_i/\lambda_0) = 0$ (no matter how electrically small), the other two defects can have arbitrary geometric and material composition without destroying perfect reflectivity. This surprising outcome does not depend on the relative location of a given set of defects due to the quasistatic nature of the EM field in the long wavelength limit.

In contrast, we now consider the same type of MIZIM and defect configuration to illustrate how incoming waves can undergo complete transmission. In Fig. 3 (a), the z-component of the magnetic field is shown as a function of position throughout the structure. The parameters are the same as previously, with only $\epsilon_{2,i}$ adjusted to satisfy vanishing of the sum in Eq. (8). The magnetic field is of course uniform in the MIZIM with standing Bessel waves in the defects. Panel (b) is the corresponding **E** field with its vector field distribution. The electric field plot shows that after the incident wave penetrates the metamaterial, it immediately becomes distorted in a

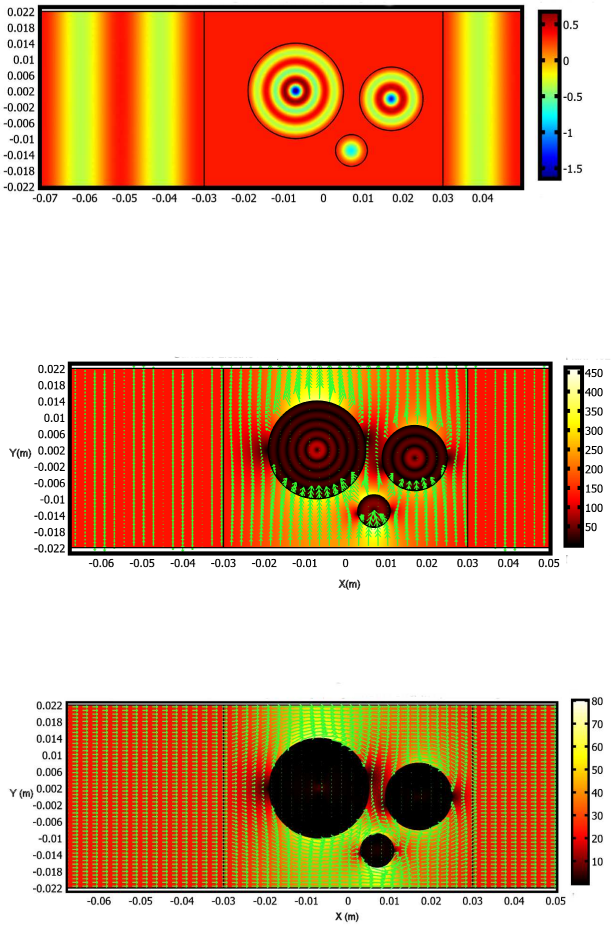

FIG. 3. (Color online) Various field profiles illustrating perfect transmission. In (a) the magnetic field pattern is shown for the same setup as Fig. 2 but with the modifications, $\epsilon_{2,1} = 9.3$, $\epsilon_{2,2} = 16.4$, and $\epsilon_{2,3} = 19.1$. In (b) the corresponding **E** field is shown. The power flow is illustrated in (c) with the Poynting vector map (time-averaged over one period) and filled contours representing its magnitude.

nontrivial fashion. Moreover, the **E** field in the defects is oriented purely in the $\hat{\phi}$ direction [see also Eq. (6)], vanishes at the boundary, and then abruptly transitions to a radial field. Just as in Fig. 2(b), the **E** field among defects exhibits a complicated spatial dependence. In Fig. 3(c), the magnitude of the (time-averaged) Poynting vector, $\mathbf{S} = c/(8\pi)\mathrm{Re}[\mathbf{E} \times \mathbf{H}^*]$, is shown with vector field overlays. The energy flow tends to "wrap around" the defects, and is compensated by higher energy flux in regions exterior to the defects to satisfy energy conservation. In all, Figs. 3(a)-(c) demonstrate the incident wave emerging from the MIZIM/defect structure in its original form. This type of structure can thus provide an

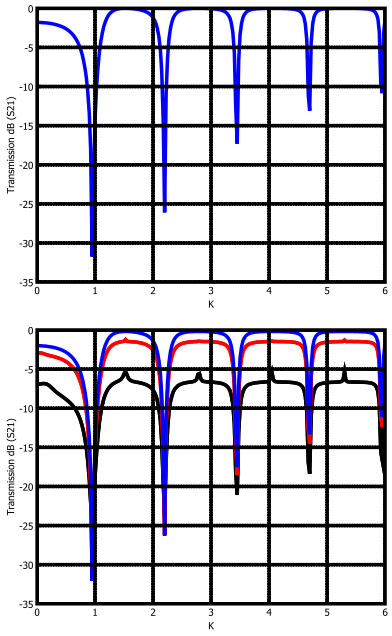

FIG. 4. (Color online) (a) Transmission (S21) versus K (see text) of the 8 mm defect for the the three defect system in Fig. 3. The effects of loss are shown in (b) for $\Gamma/\omega_p = 0.001, 0.01$, and 0.05.

alternative cloaking scenario that does not involve distorting the EM field via transformation media [26]. It also differs from the mechanism behind scattering cancellation [2]. The underlying physics resides in the long phase variation and "tunneling" effect [10] inherent to near-zero index materials. The defect's EM signatures of the impinging source wave may also serve as a type of sensor, serving as an "observation window" into the surroundings as mentioned in other contexts [2, 23].

The transmitted power as a function of the rod geometry or electrical response can yield further insight into the role that defects play in transmissivity and reflectivity enhancement crucial in the cloaking or shielding of an object. In Fig. 4(a), the transmission (S21) is plotted as a function of the material parameter, K, where $K \equiv \sqrt{\epsilon_{2,2}}$. Similar results follow for variations in the defect radius. Without loss of generality, we vary only the intermediate sized defect (8 mm). The transmission peaks coincide with the corresponding Bessel function zeros, i.e., when $J_1(k_{2,i}R_i) = 0$. Likewise, reflection dips occur where $J_0(k_{2,i}R_i)$ vanishes (as does the magnetic field in the MIZIM). Not surprisingly, incorporating a small amount of loss reduces the effect somewhat without shifting the location of the peaks (Fig. 4(b)). The close proximity of the maxima and minima in the transmission spectra might be accessible via active tuning of the defects in real-time through inclusion of liquid crystals or BaSr TiO_3, creating a potential host of reconfigurable devices [27].

In summary, we have shown through analytical calculations and numerical solutions that there exists the possibility to obtain total transmission and total reflection in MIZIMs with cylindrical dielectric defects. Remarkably, not only does the field permeate the defect, but serves as a catalyst towards perfect transmission or reflection of the incident wave, depending on the dielectric constant and radii of the defects. For shielding technologies, subwavelength defect cavities can contain elements that have the effective material parameters necessary for perfect reflection. By exploiting the quasistatic nature of the MIZIM, the complicated EM scattering that occurs in conventional materials is also avoided. Although we focused on cylindrical defects, the novel transmission characteristics outlined here can in principle be extended to different geometries.

V.C.N. and L.C. acknowledge the support from Nangyang Technological University and Ministry of Education of Singapore under Projects No. TL/SP/07-03, AcRF RG 21/07 and No. ARC 16/08. K.H. is supported in part by ONR and by a grant of HPC resources as part of the DOD HPCMP. K.H. would also like to thank J. Martin for useful discussions.

* langchen@ntu.edu.sg

[1] D. Schurig *et al.*, Science **314**, 977 (2006).
[2] A. Alú and N. Engheta, Phys. Rev. Lett. **102**, 233901 (2009).
[3] J.B. Pendry, Phys. Rev. Lett. **85**, 3966 (2000).
[4] L.V. Alekseyev and Evgenii Narimanov. Opt. Express. 14, 11184 (2006).
[5] V.G. Veselago, Sov. Phys. Usp. **10**, 509 (1968).
[6] H.-K. Yuan et al. Opt. Express **15**, 1076-1083 (2007).
[7] A. Al *et. al*, Phys. Rev. B **75**, 155410 (2007).
[8] M. Silveirinha and N. Engheta, Phys. Rev. B **75**, 075119 (2007).
[9] R.J. Pollard, *et al.*, Phys. Rev. Lett. **102**, 127405 (2009).
[10] M. Silveirinha and N. Engheta, Phys. Rev. Lett. **97**, 157403 (2006).
[11] Ruopeng Liu et al. Phys. Rev Lett. 100, 023903 (2008).
[12] B. Edwards, *et al.*, Phys. Rev. Lett. **100**, 033903 (2008).
[13] B. Edwards et al. J. Appl. Phys. **105**, 044905 (2009).
[14] K. Halterman and S. Feng, Phys. Rev. A **78**, 021805 (2008).
[15] W.G. Spitzer, *et al.*, Phys. Rev. **113**, 127 (1959).
[16] R.W. Ziolkowski, Phys. Rev. E **70**, 046608 (2004).
[17] M. A. Gingrich, and D. H. Werner, IEE Electron. Lett. **41**(23), 1266 (2005).
[18] D.-H. Kwon, *et al.*, Elec. Lett. **43** (6), 319 (2007).
[19] A. Lakhtakia, Int. J. Infrared Millim. Waves **23**, 339 (2002).
[20] A. Lakhtakia Microw. Opt. Technol. Lett **49**, 895 (2006).
[21] Z. Jiang, *et al.*, Proc. of IEEE conf. on Ant. and Prop. Society Int. Symposium (2009).
[22] J. Hao, W. Yan, and M. Qiu, Appl. Phys. Lett. **96**, 101109 (2010).
[23] G. Castaldi et al, Opt. Express, **17**, 3101 (2009).
[24] R. Pratibha *et al.*, Opt. Express **17**, 19459 (2009).
[25] COMSOL Multiphysics, http://www.comsol.com.
[26] J. Li and J.B. Pendry Phys. Rev. Lett. **101**, 203901 (2008).
[27] D.H. Werner, *et al.,* Opt. Express **15**, 3342 (2007).